Device characteristics of $CuInSe_2$-based solar cells

Jüri Krustok*, Mati Danilson, Andri Jagomägi, Maarja Grossberg, and Jaan Raudoja

Department of Materials Science, Tallinn University of Technology,
5 Ehitajate Rd., 19086 Tallinn, Estonia

ABSTRACT

Ternary chalcopyrite semiconductor $CuInSe_2$ (CIS) is a promising material for the fabrication of high-efficiency low-cost solar cells. However, various recombination losses decrease the efficiency of the cells and deteriorate their other characteristics. To identify the recombination channels and to obtain information about the related defects, we conducted current–voltage measurements at various temperatures, followed by admittance spectroscopy measurements and bias dependent quantum efficiency measurements. Two types of solar cells were studied: the ones based on the CIS monograin layers, and the others based on $CuInGaSe_2$ thin films. The temperature dependence of the open-circuit voltage of the monograin cells demonstrated that the dominant recombination channel involves CIS–CdS interface states. According to the admittance spectroscopy data, the states lie at 150–166 meV below the conduction band of CIS. In some samples, a defect state at about 45 meV was observed. The quantum efficiency measurements revealed the influence of the sulphur post-treatment on the band gap of the absorber material. The derivative curves brought out the influence in the best possible way.

Keywords: Solar cells, admittance spectroscopy, bias dependent spectral response, recombination losses, $CuInSe_2$, monograins

1. INTRODUCTION

Within the family of Cu-chalcopyrite semiconductors, $Cu(In,Ga)Se_2$ (CIGS) is of considerable interest for photovoltaic applications because of its suitable direct band gap within 1.0–1.4 eV, a high optical absorption coefficient, a moderate surface recombination velocity, and the radiation resistance.[1,2] These properties give an opportunity for the fabrication of low-cost, stable, and highly efficient thin-film solar cells. With Cu–III–VI chalcopyrite solar cells, a laboratory conversion efficiency higher than 19% has been achieved. The electrical behavior and the performance of the CIGS based thin-film solar cells depend, to a considerable degree, on the defect structure of the CdS/CIGS interface and the bulk of the depletion layer. Thus, in order to improve the properties of these heterojunction cells, a characterization of the near-interface defect levels is indispensable.

It is appropriate to mention here that a new type of solar cells based on monocrystalline $CuInSe_2$ (CIS) is under development.[3-4] These so-called monograin cells consist of very small crystallites embedded in epoxy resin. It has been shown that the isothermal recrystallization of the as-grown powder in different molten fluxes is a rather simple, inexpensive, and convenient approach to obtain suitable materials with an improved crystal structure and reduced defect concentration.[4] The resultant powders have a single crystalline grain structure, uniform chemical composition, and narrow granulometry. Due to these features, the monograin technology appears to be very promising for producing solar cells. On the other hand, there are several challenging unsolved problems related to the surface engineering of the monograin crystallites.

It is known that in the case of polycrystalline thin-film solar cells, an ordered-vacancy-compound (OVC) layer is formed on the surface of the absorber layer. The OVC layer plays an important role in determining the properties of the solar cell. The layer has been associated with the Cu–In–Se proportion of 1:3:5 and the *n*-type conductivity.[5,6]

Thin-film solar cells are fabricated mostly by the co-evaporation of elements onto Mo-coated soda lime glass. This

*E-mail: krustok@staff.ttu.ee

technology offers more opportunities for the surface layer engineering than the monograin technology. Besides, the diffusion of Na from the glass into the absorber layer can be profitably utilized in thin-film solar cells.[7] Despite the fact that the absorber material is the same, there is a number of differences as concerns the interface between CdS and $CuInSe_2$ in the thin-film and monograin solar cells. Here we draw a parallel between the cells and tackle ways and means of improving the monograin solar cells.

2. EXPERIMENTAL

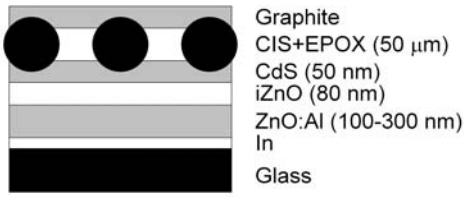

Fig. 1. Schematic cross-section of a monograin layer solar cell.

The cross-section of a monograin-layer solar cell is diagrammatically drawn in Fig. 1. The $CuInSe_2$ powder for the cells was synthesized from Cu–In and Se–In melts. More processing details can be found in Ref. 3. Subsequent to the removal of the flux, the as-grown powder was, for restoring the surface and reducing the defectiveness, post-treated in the selenium or sulphur vapor in two-zone quartz ampoules in which the vapor pressure was determined by the temperature of the Se(S) source in the low-temperature zone. The monolayer of the chemically treated powder was embedded in polyurethane (PU). CdS was deposited onto the surface of the monolayer in a chemical bath. For the cell completion, thin *i*-ZnO and conductive ZnO:Al layers were deposited by rf sputtering.

The thin-film polycrystalline CIGS solar cells were prepared at the Institute of Physical Electronics of the Stuttgart University. They are small-area (0.5 cm^2) Al:ZnO/CdS/Cu(In,Ga)Se_2/Mo/glass structures obtained by co-evaporation.

The current–voltage (*I–V*) characteristics were taken under the 100 mW/cm^2 illumination using a Keithley 2400 Source Meter. For the capacitance measurements, an Autolab Pgstat 30 FRA module working at frequencies up to 1 MHz was used. The temperature dependences were studied using a closed-cycle helium cryostat (T = 10–300 K). The quantum efficiency measurements were performed using a computer-controlled SPM-2 monochromator and a 100-W halogen–tungsten light source.

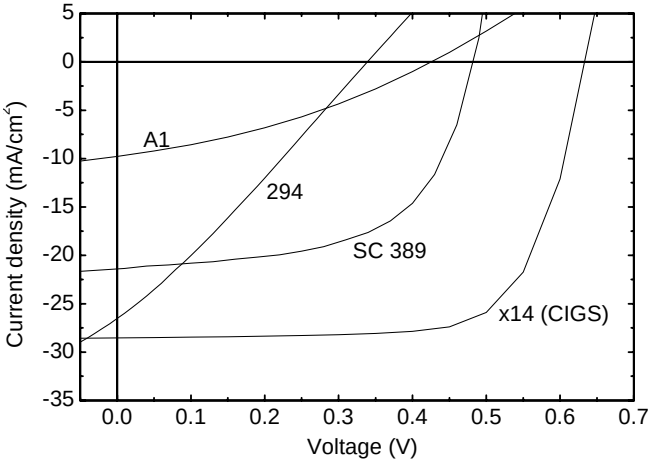

Figure 2. Current–voltage characteristics of various solar cells.

3. RESULTS AND DISCUSSION

3.1. Current–voltage measurements

The measurements showed that the *I–V* characteristics of different cells differ in a radical manner (Fig. 2). The parameters of the cells are summarized in Table 1. Sample A1 has the lowest efficiency η. A thin film CIGS solar cell has the best properties. Hence, it appears that all monograin solar cells have very high recombination losses.

It is known that the open-circuit voltage V_{oc} vs T curves are linear at RT and capable of being used for determining the main path of current losses in solar cells.[8] Each recombination mechanism contributes differently to the V_{oc} dependence. We expect that for the losses at the CdS–$CuInSe_2$ interface V_{oc} at 0 K is less than E_g/q, where E_g is the band gap energy of $CuInSe_2$ and q is the elementary charge. In this case

$$V_{\mathrm{oc}} = \frac{\Phi_b}{q} - \frac{AkT}{q}\ln\left(\frac{qS_p N_v}{j_{\mathrm{sc}}}\right), \tag{1}$$

where Φ_b is the barrier height for holes, A is the diode ideality factor, S_p is the interface recombination velocity for holes, j_{sc} is the short-circuit current density, and N_v is the effective density of states in the valence band. For bulk recombination, $\Phi_b \approx E_g$. Fig. 3 compares two different monograin solar cells. One of them exhibits the interface recombination and the other the bulk one. Consequently, the low efficiency of sample 294 is mainly caused by the interface recombination. In this case, we can expect the Fermi level pinning at the heterointerface due to the high density of the interface states. In sample A1, in which the interface recombination proves to be negligible, another loss mechanism should dominate.

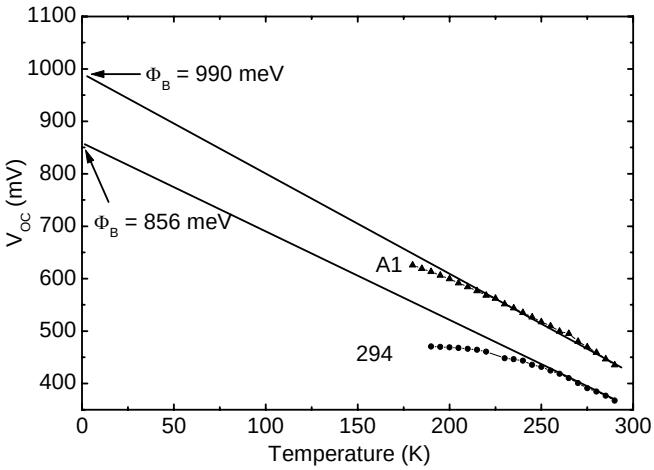

Figure 3. Extrapolation of the open-circuit voltage VB_{ocB} towards 0 K for two different $CuInSeB_{2B}$ monograin solar cells.

Sample A73 has the best characteristics among the CIS monograin cells. This is obviously related to the post-treatment of the absorber in sulphur vapor. It is known that the CIS-based monograin cells have typically lower V_{OC} and fill factor FF than the polycrystalline CIGS-based cells. One possible reason should be the high recombination rate through the interface states. Our studies show that in many cases the Fermi level is due to these states pinned at about 100–200 meV below the conduction band edge. A thin *n*-type inversion layer usually reduces the interface recombination at the CdS–CIS interface. However, the inversion of the conduction type adds new problems and does not allow exploiting the benefits of the heterojunction. Another possibility of reducing the interface recombination is the use of a material with a graded composition, so that the interface will include the material with higher E_g. Widening the band gap of the absorber reduces the spike at the absorber–buffer interface. Usually a $CuInGaSe_2$ or OVC layer is used to that end.[9] Intermixing at the interface can then help to close the recombination channel over the reduced barrier if the band discontinuity spreads over a certain distance. In monograin-layer cells, it is very difficult to form an OVC layer on the surface and, therefore, the sulphur post-treatment is used to increase the band gap at the absorber surface.

Table 1. Comparison of monograin $CuInSeB_{2\,B}$and thin-film $Cu(In,Ga)SeB_{2B}$ solar cell parameters.

Sample	Technology	Post-treatment	VB_{ocB} (mV)	JB_{sB} ($\mathrm{mA/cmP^{2P}}$)	FF (%)	η (%)
294	Monograin CIS	S	339	26.5	27.4	2.46
A1	Monograin CIS	S	425	9.8	34.27	1.42
x14	Thin film CIGS	no	633	28.5	71.78	12.95
SC389	Monograin CIS	S	481	21.4	59.08	6.08
430	Monograin CIS	S	159	4.1	33.82	0.21
434	Monograin CIS	S	253	0.1	27.72	0.0039
A73	Monograin CIS	S	420	39.5	48	8.0
A74	Monograin CIS	Se	266	17.2	29.78	1.36

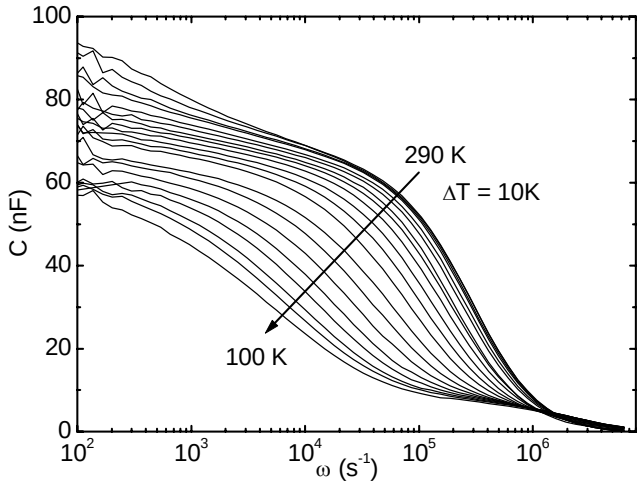

Figure 4. Capacitance–frequency curves of sample A1 taken at 100–290 K.

3.2. Admittance spectroscopy

In the admittance spectroscopy, the capacitance of a rectifying junction is investigated as a function of the frequency ω and temperature. The junction capacitance given by the depletion layer capacitance is

$$C_d = \frac{\varepsilon}{w} = \left(\frac{\varepsilon q N_a}{2V_{\mathrm{bi}}} \right)^{1/2}, \qquad (2)$$

where w is the depletion layer width, ε is the dielectric permittivity, N_a is the acceptor concentration, and V_{bi} is the built-in voltage.

The active traps in the depletion layer of the rectifying junction contribute to the capacitance spectrum at low frequencies and/or high temperatures. The effect of a single majority carrier trap on the junction capacitance can be described by[10,11]

$$C(\omega) = C_d + \frac{C_{\mathrm{lf}} - C_d}{1 + \omega^2 \tau^{*2}}, \qquad (3)$$

where C_{lf} is the low frequency capacitance which depends on the trap density N_t and the acceptor concentration N_a (if the depletion layer is in the p-type material), τ^* is the trapping time which depends on both N_t and N_a and, in addition, on w. If $N_t << N_a$, $\tau^* = 1/\omega_0$. In the small N_t limit the inflection frequency ω_0 is related to the emission rate e_t according to

$$\omega_0(T) = 2e_t(T) = 2N_{c,v} v \sigma_{n,p} \exp(-E_{\mathrm{act}} / 2kT) = 2\xi_0 T^2 \exp(-E_{\mathrm{act}} / kT), \qquad (4)$$

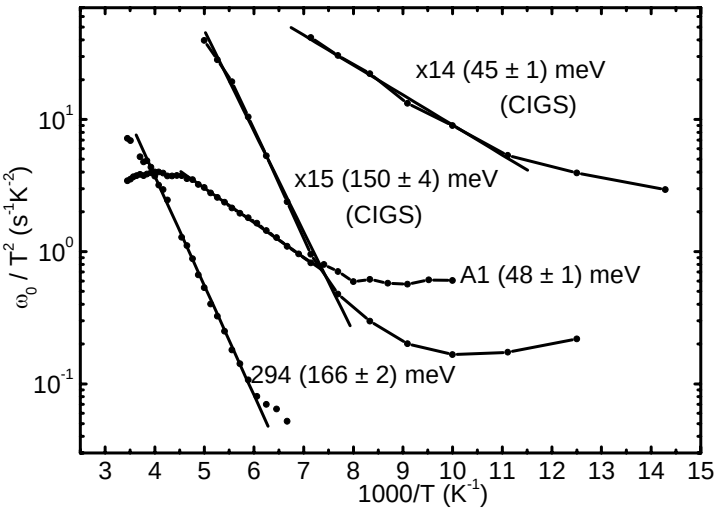

Figure 5. Arrhenius plots of the inflection frequency $\omega B_{0\mathrm{B}}$. Shown are the activation energies calculated from Eq. (4).

where $\sigma_{n,p}$ is the capture cross-section for electrons and holes, v is the electron thermal velocity at the interface, $N_{c,v}$ is the effective density of states in the conduction and valence band, and E_{act} is the activation energy of the defect level with respect to the corresponding band edge. All the temperature independent parameters are included in the emission factor ξ_0. ω_0 at each temperature can be found as a maximum of the $\omega(dC/d\omega)$ vs ω curve.

The capacitance curves of sample A1 at different temperatures are shown in Fig. 4. All the other solar cells had similar dependencies. From these curves the inflection frequencies ω_0 were found and their Arrhenius plots are shown in Fig. 5. From these plots, it is possible to find E_{act} for each sample. Typical activation energies for CIGS thin-film solar cells are 45 and 150 meV. The 150-meV activation energy is very close to the N_1 state usually observed in the CIGS solar cells.[11] The N_1 state is very likely to be an interface state.

The ac admittance spectroscopy probes the level when it coincides with the Fermi level. Fitting together the band diagram and the determined energetic position of the level, it is possible to learn about the possible spatial location of the center. From Fig. 5 it follows that in several samples there was a 45–50-meV Fermi-level-crossed defect level. The shallow energetic position of the level suggests that the electron exchange between it and the CIGS or CIS conduction band takes place in the vicinity of the heterointerface. Due to the presence of the inversion layer in the CdS–CIGS devices, this is the most probable location of the defect. Similar levels were revealed in Refs. 11 and 16. Mencaraglia *et al.*[16] showed that in the samples prepared using different CdS deposition times, a chemical surface treatment changes considerably E_{act}. It is difficult to assign any specific point defect to this level. Very probably, it involves a vacancy like ($In_{Cu}V_{Cu}$) (Ref. 17) or V_{Se} (Ref. 19). At the same time, the low activation energy may be caused by a temperature-assisted electron tunneling from the interface states to the conduction band of CdS.[18] In any event, a further research is needed to clarify the reason of the observed low activation energy.

3.2. Quantum efficiency

Quantum efficiency (QE), i.e., the ratio of the collected electrons to the incident photons, is often used to characterize the solar cell response to the light of different wavelengths. Figure 6 shows the normalized QE spectra for three cells. Sample x14 is the above-described CIGS-based thin-film solar cell. Samples A73 and A74 are prepared on the basis of the CIS monograin-layer technology. Sample A73 was post-treated in S and sample A74 in Se vapor. Consequently, the absorber of sample A73 consists of multiple layers: a layer of $CuInS_2$, a layer of $CuInSe_2$, and a changed-composition solid solution of the two in between.

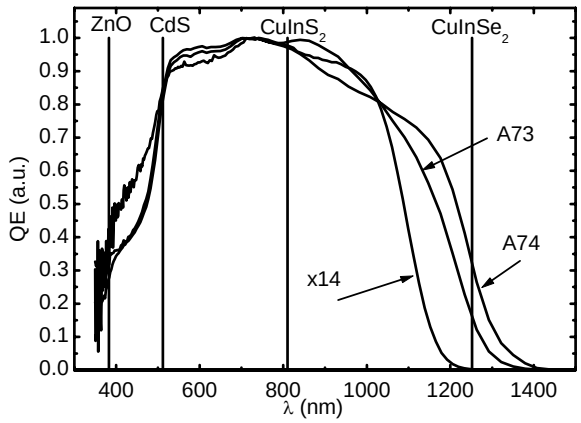

Figure 6. Normalized quantum efficiency spectra of samples A73, A74, and x14. Vertical bars indicate the approximate positions of EB_{gB} of the components.

All the three spectra have shapes typical of the solar cells of this kind. Their high-energy side is determined by the absorption in CdS and ZnO, while the low-energy side, by E_g of the absorber. The circumstance that the distance at which the photons are absorbed is greater for low-energy photons performs its role in sloping the right-hand side of the curves: the charge carriers generated have to travel a longer distance to contribute to the current and have a higher probability of recombination.

The cells compared in Fig. 6 differ in E_g of the absorber layer. As a result, in the low-energy side the spectra diverge. CIS has the lowest E_g and is capable of working with the photons of the lowest energy. Adding S into CIS increases its E_g and, therefore, the spectrum of sample A73 does not extend so far as the spectrum of sample A74. Sample x14 has the highest E_g and, thus, the shortest extension.

The low-energy side of the spectra can be fitted by the equation of Klenk *et al.*[12]

$$\mathrm{QE} = K(1-\exp(-\alpha L_{\mathrm{eff}}))\,, \tag{5}$$

where $L_{\mathrm{eff}} = w + L_d$ is the effective diffusion length of minority carriers, L_d is their diffusion length in the absorber material, and α is the absorption coefficient of the absorber material. The constant K is unity in absolute measurements.

Poor L_{eff} preventing the minority carriers from reaching the junction limits, in many cases, the efficiency of the solar cells. At the same time, Eq. (5) is not very suitable for the evaluation of L_{eff} as it requires *a priori* knowledge of α. The value of this quantity is, however, mostly unknown and often poorly measurable as, e.g., in the case of the layers with highly adsorbing monograins.

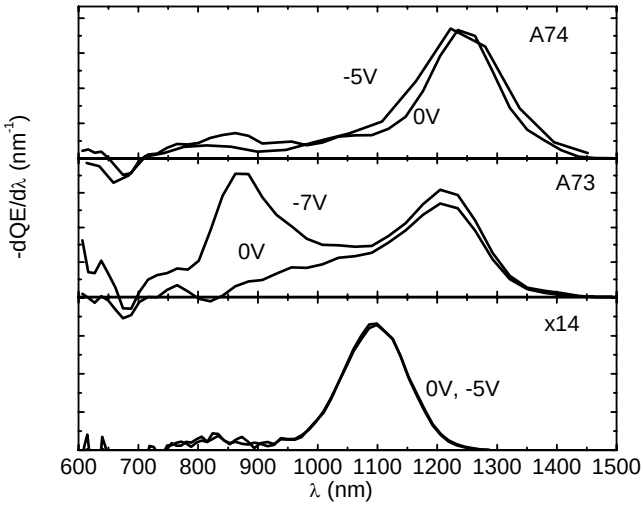

Figure 7. Derivatives of the quantum efficiency spectra for various solar cells.

The changes of QE under the bias voltage can be analyzed based on Eq. (5). Three reasons for the change are anticipated. First, reverse biasing widens the space charge region. It is believed that the collection from this region is nearly perfect. Therefore, the applied reverse voltage should increase QE. Second, biasing can alter L_d by accelerating photogenerated charge carriers. As a result, they will spend less time in the absorber and have a lower recombination probability. Third, the applied voltage can change the absorption coefficient. The latter, not a particularly strong idea stems from the observations that the laser-induced electric field can change the optical properties of a material.

The form of the QE spectra of the monograin-layer solar cells depended on the bias voltage. This is a sign of a too short carrier diffusion length.

Figure 7 shows the derivatives of the QE spectra of the same samples as in Fig. 6. For each sample, the measurements were carried out at two biasing voltages. As seen, the derivative spectrum of sample A74 has one Gaussian peak regardless of the applied voltage. For sample A73 one peak at 0 V and two Gaussian peaks at –7 V were registered. In the case of sample x14, the look with one peak remained totally unchanged in the voltage range of 0 to –5 V.

There is a reasonable agreement between the maxima of the derivative spectra and the values of E_g of the absorber. So, the measured peak position for sample A74 (1250 nm) corresponds very well to the band gap energy of $CuInSe_2$. For sample A73, the left-hand peak has a position at a slightly lower energy than E_g of pure $CuInS_2$; the shift seems to be caused by the incorporated Se. On the contrary, the right-hand peak has the position at a slightly higher energy than E_g of $CuInSe_2$, with the shift caused by the incorporated S.

Note that in the case of solids with a large concentration of native defects as we have,[13,14] function $\alpha(E)$ that determines the shape of the low-energy side of the QE spectra can be approximated as $A(E - E_g)^{1/2}/E$, where A is a constant, if $E > E_g$ (E_g is here for the band gap energy of the perfect direct gap material), and as[15] $B(E_0\zeta_p^{1/2}\exp((E - \zeta_p)/E_0))$, where B is a constant and ζ_p and E_0 are the characteristic parameters of the material that increase with the doping level, if $E < E_g$. Hence, $\alpha(E)$ changes slower in the latter region, and the appearance of the inflection in the QE spectra and the maximum in the derivative spectra are expected.

4. CONCLUSIONS

The properties of CIS monograin-layer solar cells were investigated by admittance spectroscopy and the measurement of the quantum efficiency spectra and current–voltage characteristics. It follows from the temperature dependence of the open-circuit voltage that the dominating recombination channel involves the CIS–CdS interface states. The admittance spectroscopy revealed two types of levels with the activation energies of 150–166 meV and 45–48 meV. The deeper level is most probably caused by the interface states, while the shallow one, by the bulk defects. A post-treatment in sulphur vapor was shown to increase the band gap at the absorber surface and the open-circuit voltage. However, the quantum efficiency measurements showed a poor carrier collection. The derivative quantum-efficiency spectra taken under various biasing brought out the influence of the sulphur treatment in the best possible way.

ACKNOWLEDGMENT

The financial support of the European Commission through the program "Energy, environment, and sustainable development" and the Estonian Science Foundation (Grant No. 5149) is gratefully acknowledged. We thank our colleagues from the Institute of Physical Electronics of the Stuttgart University for the preparation of the CIGS thin-film solar cells and Dr. M. Igalson from the Warsaw University of Technology for helpful discussions.

REFERENCES

1. J. E. Jaffe and A. Zunger, "Theory of the band-gap anomaly in ABC_2 chalcopyrite semiconductors", *Phys. Rev. B* **29**, pp. 1882–1906, 1984.
2. M. Yamaguchi, "Radiation resistance of compound semiconductor solar cells", *J. Appl. Phys.* **78**, pp. 1476–1480, 1995.
3. M. Altosaar and E. Mellikov, "$CuInSe_2$ monograin growth in CuSe–Se liquid phase", *Jpn. J. Appl. Phys.* **39**, Suppl. 39-1, pp. 65–66, 2000.
4. M. Altosaar, A. Jagomägi, M. Kauk, M. Krunks, J. Krustok, E. Mellikov, J. Raudoja, and T. Varema, "Monograin layer solar cells", *Thin Solid Films* **431**–**432**, pp. 466–469, 2003.
5. D. Schmid, M. Ruckh, F. Grunwald, and H. W. Schock, "Chalcopyrite/defect chalcopyrite heterojunctions on the basis of $CuInSe_2$", *J. Appl. Phys.* **73**, pp. 2902–2909, 1993.
6. M. Turcu, O. Pakma, and U. Rau, "Interdependence of absorber composition and recombination mechanism in Cu (In, Ga)(Se, S)$_2$ heterojunction solar cells", *Appl. Phys. Lett.* **80**, pp. 2598–2600, 2002.
7. S.-H. Wei, S. B. Zhang, and A. Zunger, "Effects of Na on the electrical and structural properties of $CuInSe_2$", *J. Appl. Phys*. **85**, pp. 7214–7218, 1999.
8. M. Schmidt, D. Braunger, R. Schäffler, H. W. Schock, and U. Rau, "Influence of damp heat on the electrical properties of Cu(In,Ga)Se_2 solar cells", *Thin Solid Films* **361**–**362**, pp. 283–287, 2000.
9. Y. Okano, T. Nakada, and A. Kunioka, "XPS analysis of CdS/$CuInSe_2$ heterojunctions", *Sol. Energy Mater. Sol. Cells* **50**, pp. 105–110, 1998.
10. A. Niemegeers, M. Burgelman, R. Herberholz, U. Rau, D. Hariskos, and H.-W. Schock, "A model for the electronic transport in Cu(In,Ga)Se_2 solar cells", *Prog. Photovolt. Res. Appl.* **6**, pp. 407–421, 1998.
11. R. Herberholz, M. Igalson, and H. W. Schock, "Distinction between bulk and interface states in $CuInSe_2$/CdS/ZnO by space charge spectroscopy", *J. Appl. Phys.* **83**, pp. 318–325, 1998.
12. R. Klenk and H. W. Schock, "Photocurrent collection in thin film solar cells – calculation and characterization for $CuGaSe_2$/(Zn,Cd)S", In *Proc. 12th Euoropean Photovoltaic Solar Energy Conf.,* pp.1588-1591, 1994.
13. J. Krustok, H. Collan, M. Yakushev, and K. Hjelt, "The role of spatial potential fluctuations in the shape of the PL bands of multinary semiconductor compounds", *Phys. Scripta* **T79**, pp. 179–182, 1999.
14. J. Krustok, J. Raudoja, M. Yakushev, R. D. Pilkington, and H. Collan, "On the shape of the close-to-band-edge photoluminescent emission spectrum in compensated $CuGaSe_2$", *Phys. Status Solidi A* **173**, pp. 483–490, 1999.
15. J. I. Pankove, "Absorption edge of impure gallium arsenide", *Phys. Rev.* **140**, pp. A2059–A2065, 1965.
16. D. Mencaraglia, S. Ould Saad, and Z. Djebbour, "Admittance spectroscopy for non-crystalline thin film devices characterization: comparison of Cu(In,Ga)Se and a-Si:H cases", *Thin Solid Films* **431**–**432,** pp. 135-142, 2003.
17. S. B. Zhang, S.-H. Wei, and A. Zunger, "Defect physics of the $CuInSe_2$ chalcopyrite semiconductor", *Phys. Rev. B* **57,** pp. 9642–9656, 1998.
18. P. Zabierowski and M. Igalson, "Thermally assisted tunnelling in Cu(In,Ga)Se_2-based photovoltaic devices", *Thin Solid Films* **361–362**, pp. 268–272, 2000.
19. P. Zabierowski, U. Rau, and M. Bodegard, "Laplace-DLTS analysis of the minority carrier traps in the Cu(In,Ga)Se_2-based solar cells", *Eur. Mater. Res. Soc. Symp. Proc*., to be published.